catalysts

MDPI

Article

TiO_2 Nanotubes Supported Cu Nanoparticles for Improving Photocatalytic Degradation of Simazine under UV Illumination

Syazwan Hanani Meriam Suhaimy [1,2], Sharifah Bee Abd Hamid [1,*], Chin Wei Lai [1], Md. Rakibul Hasan [1] and Mohd Rafie Johan [1]

[1] Nanotechnology and Catalysis Research Center, University of Malaya, 50603 Kuala Lumpur, Malaysia; hanani_ms@yahoo.com.my (S.H.M.S.); cwlai@um.edu.my (C.W.L.); rakibacctdu@gmail.com (M.R.H.); mrafiej@um.edu.my (M.R.J.)

[2] Faculty of Science, Technology and Human Development, Universiti Tun Hussein Onn Malaysia, UTHM, Parit Raja, 86400 Batu Pahat, Malaysia

* Correspondence: sharifahbee@um.edu.my; Tel.: +60-37-967-6959; Fax: +60-37-967-6956

Academic Editor: Dionysios (Dion) Demetriou Dionysiou
Received: 15 August 2016; Accepted: 21 October 2016; Published: 29 October 2016

Abstract: Nano size Copper (Cu) incorporated TiO_2 nanotubes was successfully synthesized via the anodic oxidation technique in ethylene glycol (EG) containing 0.5 wt % NH_4F and 1.6 wt % KOH for the photocatalytic degradation of Simazine (2-chloro-4, 6-diethylamino-1,3,5-triazine) under Ultraviolet (UV) illumination. In the present study, the influence of different loading Cu concentrations on the formation of Cu-TiO_2 nanotubes film towards the photocatalytic degradation of Simazine is reported. Based on our study, it was found that the optimum Cu loading concentration was about 0.45 wt % on TiO_2 nanotubes film for approximately 64% photocatalytic degradation of Simazine after 4 h under UV illumination. This finding was mainly attributed to the uniform surface covering of the Cu loaded TiO_2NTs which acted as electron traps, preventing the recombination of electron hole pairs, eventually leading to higher photocatalytic activity of our photocatalyst in degrading the targeted organic pollutant, Simazine. Moreover, an increased kinetic rate of the degradation to 0.0135 h^{-1} was observed in the presence of Cu in TiO_2NTs.

Keywords: TiO_2; cuprous oxide; photocatalyst; anodization; Simazine; photocatalytic

1. Introduction

Various applications of herbicides and pesticides as a habitual practice to increase agricultural productivity has resulted in an unintended impact to the environment. One major issue with herbicides is the ability to leach into groundwater systems which are then used as drinking water sources [1]. Among the herbicides, Simazine (6-chloro-*N*,*N*′-diethyl-1,3,5-triazine-2,4-diamine, SMZ), is popularly used to control the growth of annual grasses and broad leaf plants. The U.S. Environmental Protection Agency (EPA) classified Simazine as one of the five herbicides which has frequency of occurrence thus having potential to pollute groundwater [2]. Simazine is widely detected in groundwater systems due to its poor biodegradability. The resistance of Simazine to detoxify with conventional treatment methods can lead to major environmental problems and is suspected of being an endocrine disruptive effect chemical [3]. Therefore, numerous studies have been carried out such as by photocatalysis [4], Fenton's oxidation [2], UV photolysis [5], and biological methods [6] to develop an effective and efficient treatment method for SMZ's removal from water and the soils concerned [7]. Titanium dioxide (TiO_2) is a superior photocatalyst with promising application in water treatment and has become the most studied photocatalytic material used to degrade organic compounds [8]. Owing to its outstanding chemical and physical properties such as high chemical stability, high catalytic activity,

ease of availability, and non-toxic behavior, TiO_2 is feasible for extensive application in catalysis, energy storage, sensing etc [9–12]. However, TiO_2 absorbs only UV light corresponding to its wide band gap value of 3.0–3.2 eV which restricts its technological use. As a matter of fact, the anatase phase of TiO_2 can only absorb UV light for photocatalytic activation. Improving the optical properties by narrowing the band gap of TiO_2 would give a positive impact on the photodegradation ability [7,13].

Table 1 shows that the percentage of Simazine degradations are not 100% even after 7 h of degradation time. Therefore our study was to fabricate electrolyte forming TiO_2 nanotubes to enhance Simazine degradation or TiO_2 photocatalyst activity under UV illumination. From the literature, many researchers have focused on TiO_2 nanoparticles (Degussa P25) [4,14]. However this is subject to higher cost, and may undergo aggregation as a result of nanosized instability [15,16]. In contrast, in this work, we synthesized TiO_2 in the form of nanotubes. This method provides advantages in controlling the highly ordered, self-oriented, homogeneous characteristics of the material and is cost effective. Recently, Wang et al. [17] reported a degradation of Rhodamine B by Cu-doped TiO_2 photocatalyst, however the ultrasonication-assisted sequential chemical bath deposition method possessed disadvantages such as lack of reproducibility and inefficiency in converting the precursor materials into useful deposits [18], thus restricting practicality in industrial application. The formation of our TiO_2NTs was further enhanced by incorporation of alkali-species into ethylene glycol (EG) during the anodic oxidation process [19]. In 1996, Morawski et al. [20] reported that using potassium leads to a more active TiO_2 catalyst. Additionally, due to the reason that the high rate of chemical dissolution in fluoride containing electrolyte could limit the nanotube length, additives such as potassium hydroxide (KOH) were added to the electrolyte solutions to reduce the dissolution rate of TiO_2 formed [21]. KOH is a strong base and is totally dissociated in water as shown in Equation (1). The presence of potassium ion (K^+) derived from the electrolyte is expected to result in adsorbtion on the titanium dioxide nanotubes' (TiO_2NTs) surface. This will enhance the overall TiO_2NTs photocatalytic efficiency owing to the reason that KOH is an efficient activating agent in generating nanotube porosity compared to other alkaline hydroxides. K^+ can be intercalated in all different types of nanotubes and thus is responsible for the development of microporosity [22].

$$KOH + H_2O \rightarrow K^+ + OH^- \quad (1)$$

Table 1. The percentage of Simazine (SMZ) degradation obtained by TiO_2 photocatalyst.

Year	Preparations Methods Materials Light Source	Results	References
2011	Photolysis SMZ concentration (5 ppm), TiO_2 concentration (0.05 to 0.25 g/L) Mercury lamp	No full mineralization of SMZ was achieved 25% SMZ degradation after 1 h Cyanuric acid present as final product Pseudo first order	Munoz et al. [25]
2014	Sonocatalytic, Photocatalytic, Sonophotocatalytic SMZ concentration (5 ppm), Au-TiO_2 concentration (0.2 g/L to 3.0 g/L) Visible light	Order if degradation of SMZ after 7 h degradation (Sonophotocatalysis, 43% > Sonocatalysis, 31% > Photocatalysis, 26%) 1.5 g/L is the optimum Au-TiO_2 concentration Pseudo first order	Sathishkumar et al. [7]
2013	Ultrasonication-assisted sequential chemical bath deposition 0.14 g Copper acetate Cu_2O loaded TiO_2 Visible light	Rhodamine B degradation After 19 min, 24.96% Cu_2O/TiO_2 of RhB degraded Photoelectrocatalysis, 84.29% > electrocatalysis, 41.07% > photocatalysis, 5.00% > selfdegradation, 1.45% Pseudo first order	Wang et al. [17]
2013	SMZ concentration (0.06 ppm) Degussa P25 (0.05 to 0.80 g/L) H_2O_2 (4 mM) Visible light	Optimum condition (pH 6.5, TiO_2 0.1 g/L, [H_2O_2] 4 mM, 0.5 mM Cr(VI) In 20 min, >97% of SMZ degraded with the presence of Cr(VI), 120 min to achieve without Cr(VI)	Rao et al. [14]
2009	SMZ concentration (0.025 mM), Degussa P25 (0.1 g/L) UV light	Optimum condition (pH 9, TiO_2 0.1 g/L) Pseudo first order	Chu et al. [4]

However, in order to increase the photocatalytic efficiency, it is also essential to ensure that the electron-hole pairs can move to the surface reaction sites of the semiconductor after they become excited from Valence Band (VB) to Conduction Band (CB) before they recombine in bulk. Other than that, toxicologically innocuous and environmentally benign media [23] for chemical reactions such as ethylene glycol (EG) were also used in the electrolyte. The addition of EG to the electrolyte which acts as a reducing agent and stabilizer could inhibit the reduction reaction during the electrodeposition process [24]. To the best of our knowledge, detailed studies on TiO_2NTs via anodization and their SMZ photodegradation performance are lacking. In this work, Cu was used to prepare TiO_2NTs in the presence of KOH electrolyte to overcome the drawbacks such as recombination losses of charge carriers and to enhance the photocatalytic ability in photocatalytic degradation application. This study aims to determine the optimum Cu concentration in TiO_2NTs for the best SMZ photocatalytic degradation performance.

2. Results and Discussion

2.1. SEM Analysis

The surface structural changes of anodized samples were observed by SEM. Before the addition of Cu into the electrolyte solution, the nanotubes formations are disorganized as shown in Figure 3a. However, with the addition of 0.45 wt % of Cu, vertically ordered open ended tubes of TiO_2 were formed as shown in Figure 1b. From the cross-section views of this sample, it can be seen that the nanotube arrays are parallel aligned, length in the range of 1.22 μm with the highest aspect ratio of 14.59 (Figure 2). The surface modification of TiO_2NTs with Cu can affect its optical and photocatalytic activities [17]. The tubular structure provides superior photocatalytic ability due to a large surface area, and facilitates the absorption of SMZ into the TiO_2NTs surface [26]. The structural morphology of samples changed significantly for a higher amount of Cu. However, no porosity and vertically oriented structure of nanotubes were formed on increasing the amount of Cu as shown in Figure 1c–e. Meanwhile, part of the tubular structure of TiO_2NTs was distinctly damaged at 1.35 wt % of Cu due to collapsing and became very non-uniform. Table 2 shows the details of texture properties for all samples.

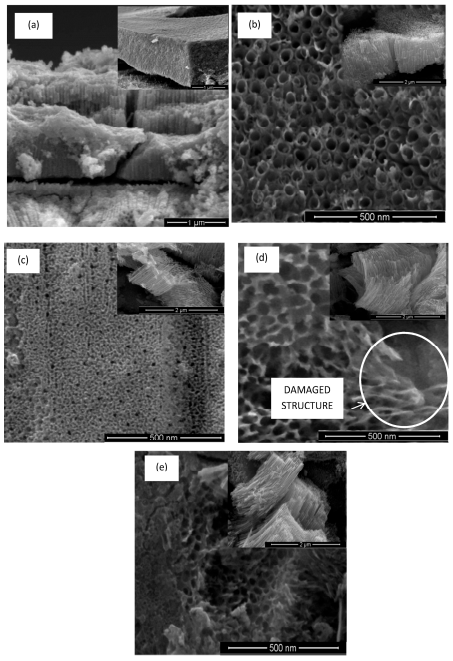

Figure 1. Scanning electron microscopy (SEM) images of TiO_2NTs for (**a**) Cu-00; (**b**) Cu-01; (**c**) Cu-02; (**d**) Cu-03, and (**e**) Cu-04.

Table 2. Geometrical dimension of all samples.

Parameters	Cu-00	Cu-01	Cu-02	Cu-03	Cu-04
Length of tube, L (nm)	1288.0	1220.0	667.0	556.0	334.0
Pore Size, D (nm)	37.5	68.7	49.0	48.0	44.5
Wall thickness, W (nm)	33.4	7.3	10.3	8.5	4.4
Interpore distance, A (nm)	77.2	72.5	73.3	68.6	49.5
Aspect ratio, R	12.3	14.6	9.6	8.6	6.3
Geometric surface area factor, G	61.9	97.9	60.2	54.9	42.7

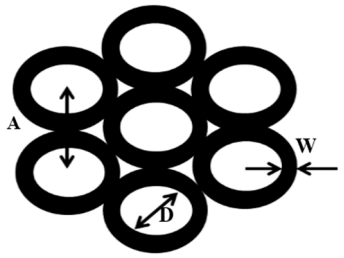

Figure 2. Idealized geometric relationships in hexagonal nanotubular array with a wall thickness (W), interpore distance (A), and pore size (D).

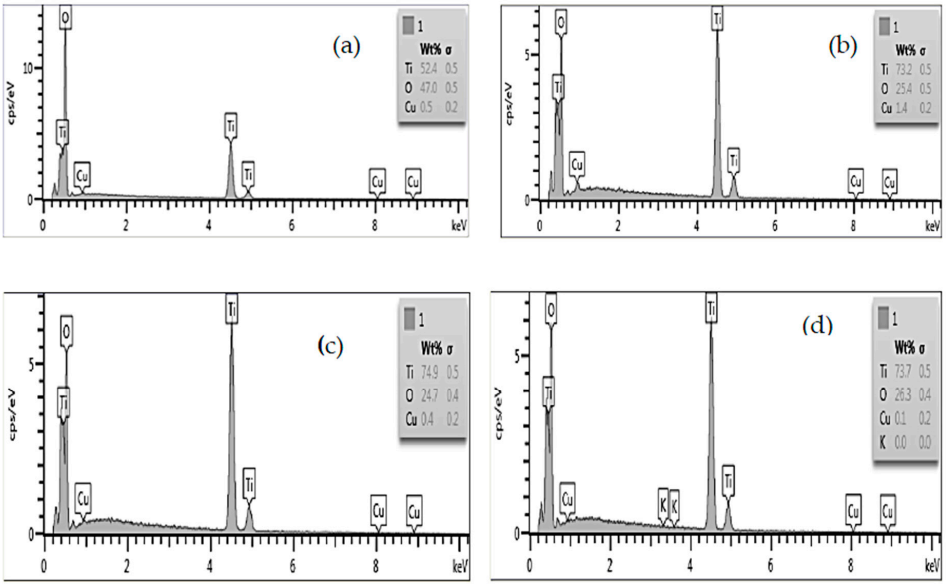

Figure 3. Energy dispersive X-ray spectroscopy (EDX) spectra of (**a**) Cu-01; (**b**) Cu-02; (**c**) Cu-03; (**d**) Cu-04.

2.2. Elemental Analysis

It is clearly seen that the synthesized films are mainly composed of Cu, Ti, and O elements, as shown in Table 3. As seen in the EDX spectra above (Figure 3), no other peak related to impurity was detected from the elemental composition. This confirms that only copper has been incorporated onto the TiO_2 surface.

Table 3. Energy dispersive X-ray spectroscopy (EDX) analysis of all samples.

Sample	Element	wt %	atomic %
Cu-00	Ti	56.62	30.35
	O	43.38	69.95
Cu-01	Ti	52.45	27.08
	O	47.04	72.72
	Cu	0.51	0.20
Cu-02	Ti	73.20	48.73
	O	25.36	50.55
	Cu	1.43	0.72
Cu-03	Ti	74.90	50.18
	O	24.75	49.64
	Cu	0.36	0.18
Cu-04	Ti	73.66	48.33
	O	26.28	51.63
	Cu	0.06	0.03

Figure 4 shows the current density-time transients during 30 min anodization time. Clearly a different current density is obtained by varying the electrolyte composition indicating a significant difference in the nanotubes growth behavior. As for samples labelled Cu-02, Cu-03, and Cu-04, the current density value becomes 0 even after 6 min anodization time has been observed. Thus, this hindered the ionic transport across the oxide/electrolyte interface, resulting in slow growth of the initial oxide layer. However, for sample Cu-01, the current density value was found as ~2.0 $mA \cdot cm^{-2}$ throughout the 30 min anodization time. This shows a large amount of charge carrier transport at the metal/electrolyte interface which further accelerates chemical dissolution and thus induces the formation of a thick initial oxide layer. The results suggest that Cu concentration has a big influence on the growth behavior, which eventually determines the $CuTiO_2$NTs morphological characteristics as is shown in the previous SEM results.

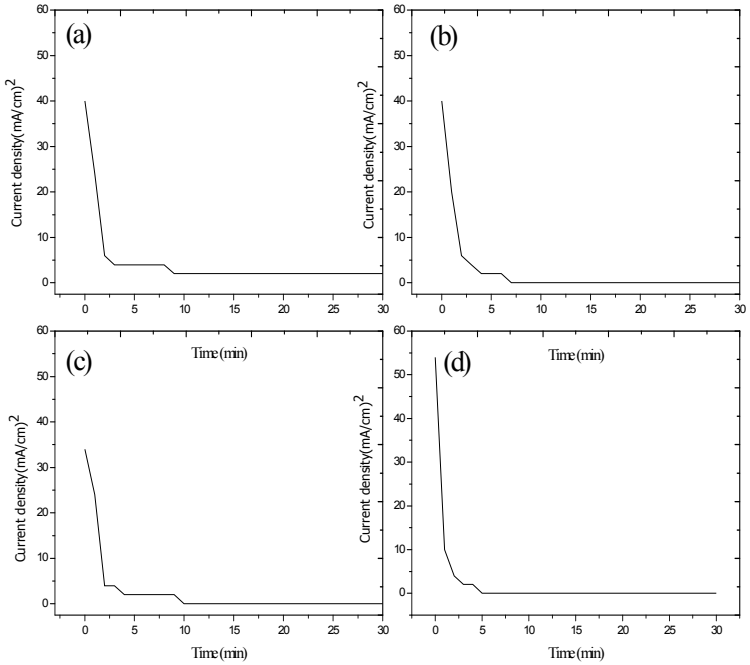

Figure 4. Current-density time response of $CuTiO_2$NTs samples anodized using different Cu-loadings in EG- electrolytes labelled (**a**) Cu-01; (**b**) Cu-02; (**c**) Cu-03; (**d**) Cu-04.

2.3. XRD Analysis

Figure 5 shows the XRD patterns of the pure TiO_2NTs and $CuTiO_2$NTs film annealed at 450 °C in 2 h. It is observed that peaks at angles of 25.64, 38.40, 40.37, 53.42, 63.22, 71.02, and 76.62 have diffractions by planes (101), (004), (112), (105), (213), (220), and (107), respectively. These diffractions were attributed to the presence of anatase phase which is predominant in the sample (ICSD 01-075-1537). The Ti peaks originated from the Ti metallic substrate with lattice parameters of a = 0.37 nm, b = 0.37 nm, and c = 9.37 nm. TiO_2 are found to display tetragonal coordination. After being doped with Cu, the geometric arrangement changed to hexagonal with lattice parameters a = 0.30 nm, b = 0.30 nm, and c = 11.44 nm. Therefore, it is reasonable to suggest that Cu atoms influence the crystal structure. The average crystallite sizes of the particles are calculated by Scherer's equation [27], which are 143.5 nm for pure TiO_2 and 42.9, 87.7, 35.6, and 33.7 nm for samples Cu-01, Cu-02, Cu-03, and Cu-04, respectively. However, the resulting spectrum shows that there has been a decrease in intensity for the sample labelled Cu-04. It is clear that the anodization at higher loading of Cu induces an abrupt change in the crystalline structure. This result is in good agreement with SEM images. Although a greatly differing intensity is observed for that sample, the main peaks correspond to a titanate phase. Furthermore, copper(I) oxide (Cu_2O) may not be able to exhibit any diffraction pattern in the above spectra owing to the fact that the Cu component is highly dispersed in samples due to the low quantity of copper loading below the XRD detection limit.

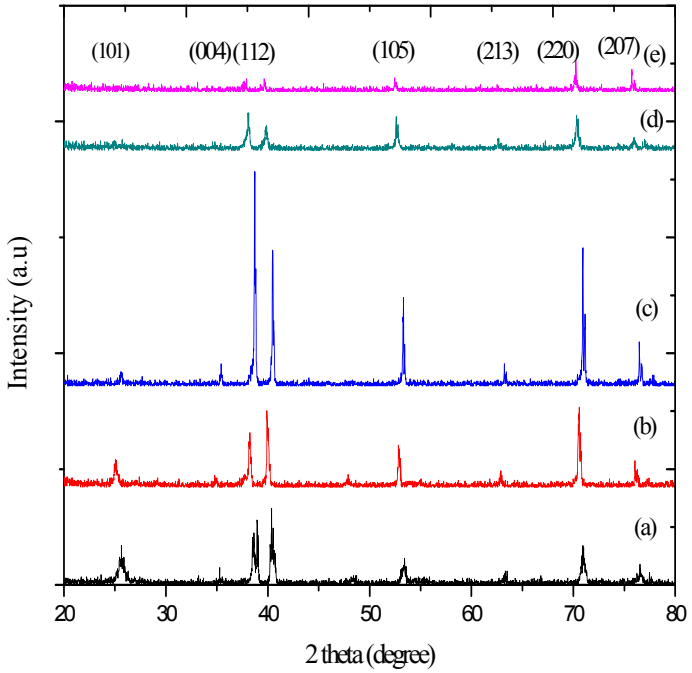

Figure 5. X-ray Diffraction (XRD) patterns of $CuTiO_2$ photocatalyst labelled (**a**) Cu-00; (**b**) Cu-01; (**c**) Cu-02; (**d**) Cu-03; and (**e**) Cu-04.

2.4. Raman Analysis

Figure 6 displays the Raman spectra of TiO_2NTs and $CuTiO_2$NTs. The presence of fundamental vibrational modes of anatase Eg_1, Bg_1, Ag_1 + Bg_1, and Eg_3 at 144, 395, 514, and 639 cm^{-1}, respectively [28]. According to the above spectra, no relative shifts of vibration modes to higher wavenumber amongst the doped samples were observed. However, significant difference in intensity and peak broadening of the vibrational modes were observed. This is due to the surface disorder as a result of oxygen vacancies (nonstoichiometry defects) and atomic interaction –Ti–O–Cu– [28]. Doping TiO_2 generates oxygen vacancy which is believed to distort the symmetry of the peak to cause

broadening [29]. Furthermore, this confirms that the oxygen vacancies are greater when the TiO_2 lattice is doped by a Cu atom with greater broadening compared to pure TiO_2. This indicates the successful doping and uniform distribution of the metal ions in the titanium ion sites.

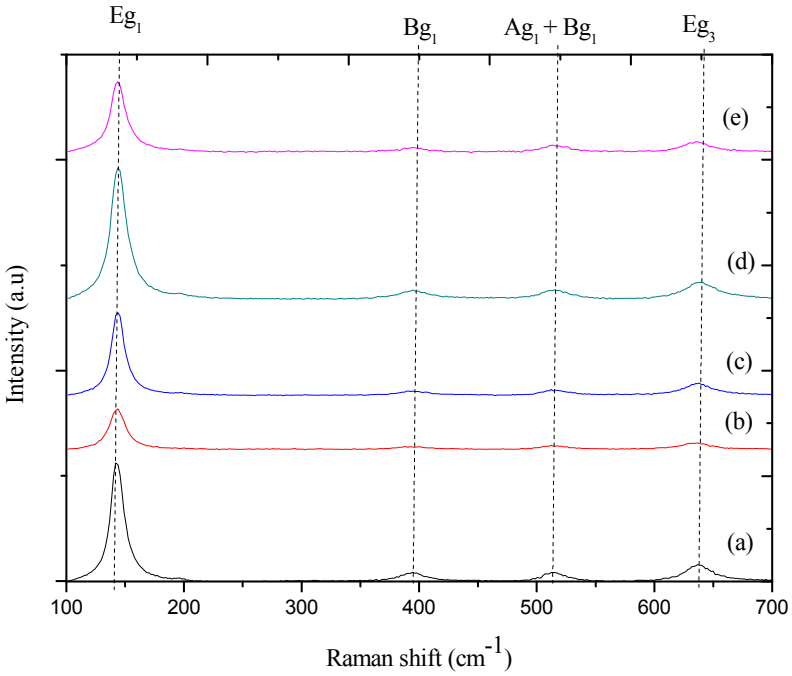

Figure 6. Raman spectra showing peaks for samples (**a**) Cu-00; (**b**) Cu-01; (**c**) Cu-02; (**d**) Cu-03; and (**e**) Cu-04.

2.5. XPS Analysis

The XPS analysis of sample Cu-01, which showing the best structural morphology was employed to study the chemical nature and surface changes after copper deposition. The survey spectra are shown in Figure 7 containing the peaks of Ti2p, O1s, and Cu2p. There are two Ti2p peaks with binding energies at around 458.7 and 464.3 eV that are assigned to $Ti2p_{3/2}$ and $Ti2p_{1/2}$, respectively which suggests that Ti exists mostly in the form of Ti^{4+} [30–32]. The result shows that the $Ti2p_{1/2}$ component is broader than the $Ti2p_{3/2}$ peak caused by the Coster-Kronig effect [33]. The occurrence of post-ionization, $Ti2p_{3/2}$ state is long lived compared to the $Ti2p_{1/2}$ state. In addition three peaks centered at 528.6, 529.9, and 531.4 eV in the O 1s spectrum are observed. According to the literature, the binding energy at 529.9 eV shows characteristic signals due to Ti-O and at 531.9 eV the oxygens are in the form of hydroxyl groups [34]. It should be noted that the peak at 933.5 eV was assigned to Cu 2p in a form of Cu(I) oxide [35,36]. Since the atomic radius of Cu (135 pm) is smaller than Ti (140 pm), the Cu^+ ion could be substituted into the lattice of TiO_2 forming a Ti–O–Cu linkage. Moreover, Cu(1.90) has a higher electronegativity than Ti(1.54) which further becomes a factor for a successful doping into the interstitial TiO_2 structure [37]. Furthermore, XPS data demonstrated no presence of other elements, revealing no contaminations exist on the surface. This observation was further supported and in a good agreement with EDX results. Based on the XPS results, it can be inferred that Cu exists in a form of Cu^+ oxidation state.

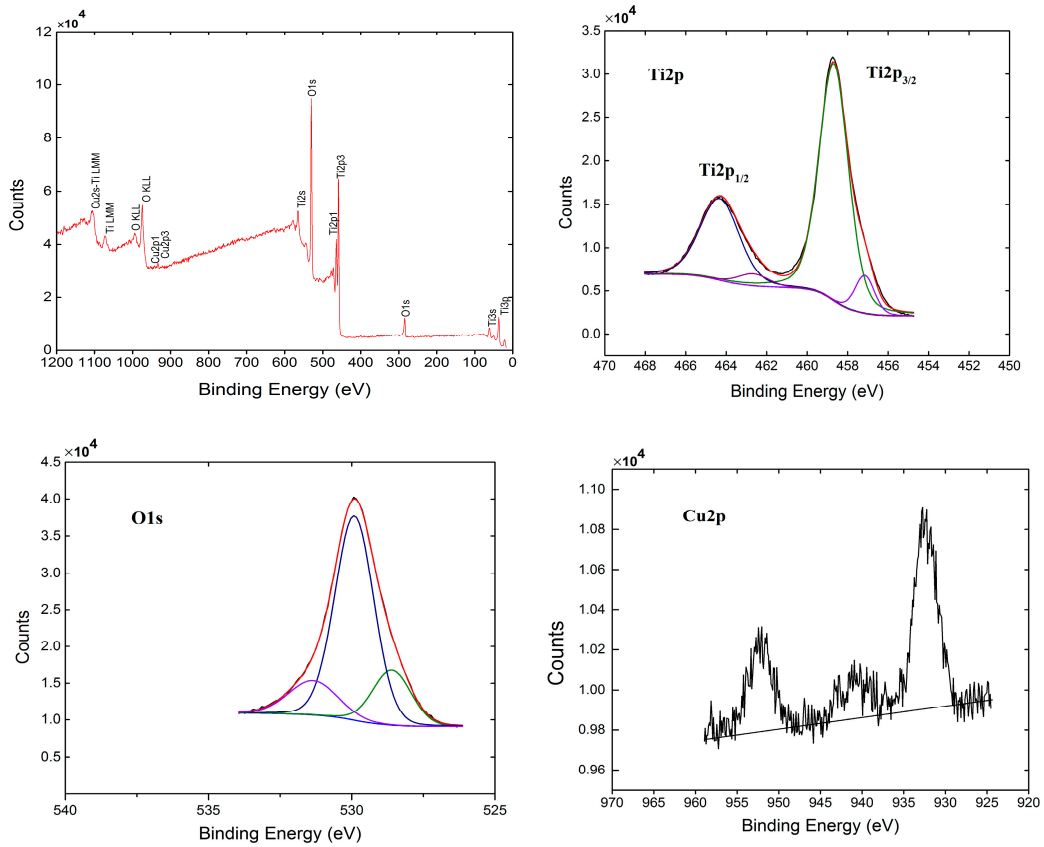

Figure 7. X-ray photoelectron spectroscopy (XPS) spectra of $CuTiO_2$NTs labelled Cu-01.

2.6. TEM Analysis

The incorporation of Cu(I) oxide was further proved by Transmission Electron Microscopy (TEM) and Energy Dispersive X-ray Spectroscopy (EDS) as shown in Figures 8 and 9. The sample contains Cu, Ti, and O, and no other elements were observed. TEM images clearly show Cu nanoparticles substituted inside the tubes revealed by the presence of a Cu(I) oxide component. In addition, Cu(I) oxide was also deposited on the outer wall of the tubes as the surface of the nanotube is rough.

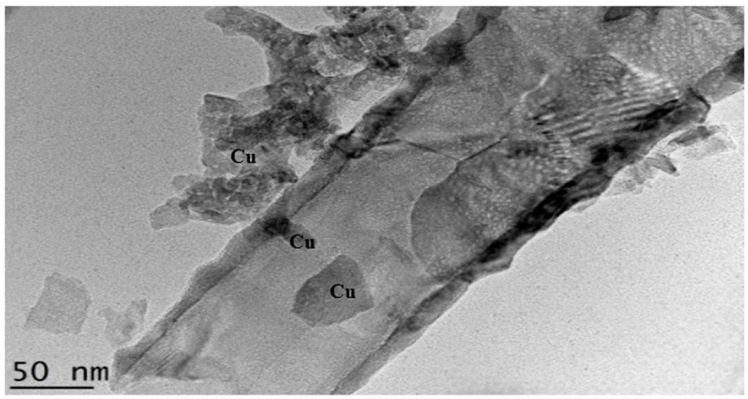

Figure 8. Transmission electron microscopy (TEM) image shows cross sectional morphologies of $CuTiO_2$NTs labelled Cu-01.

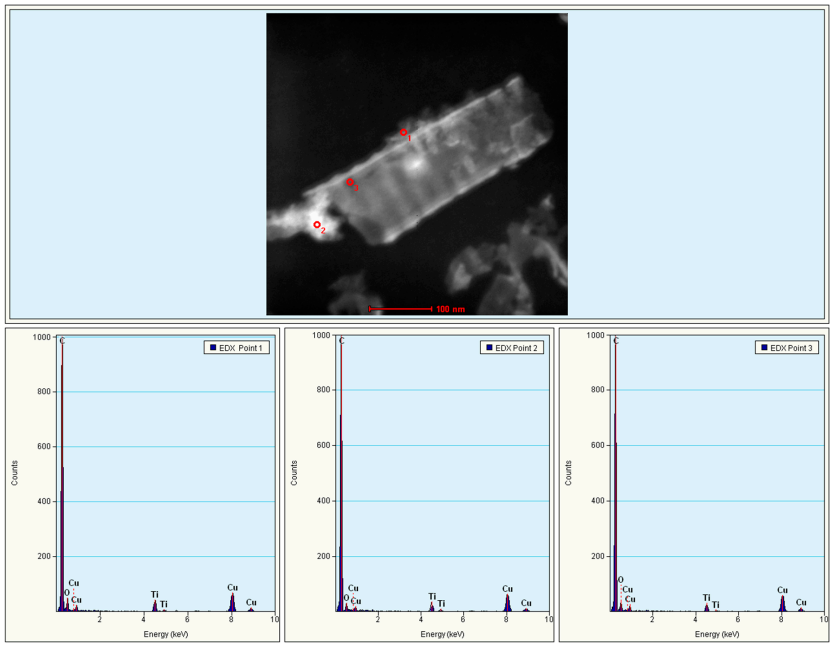

Figure 9. Energy dispersive x-ray spectroscopy (EDS) of $CuTiO_2$NTs labelled Cu-01.

2.7. Photoluminescence (PL) Analysis

The PL measurement was performed in order to further understand the presence of surface defects and the emission properties of the sample. The PL spectra of all samples excited in the wavelength range of 400 nm to 700 nm are shown in Figure 10. Blue shift was observed from the PL emission where wider light absorptions were above 500 nm [38]. This wavelength shifts positively when Cu is added into TiO_2 suggesting increased crystalline defects within the TiO_2 structure. The PL signal arises from the defects associated with oxygen vacancies [39]. In PL spectra, the higher emission intensity is indicative of a higher recombination of photo-excited electron and holes [40]. From the above results, it can be seen that TiO_2 exhibits higher emission intensities than that of all $CuTiO_2$NT samples. Thus, it indicates that Cu incorporated in TiO_2 may have a higher electron–hole separation efficiency compared with the pure TiO_2 sample.

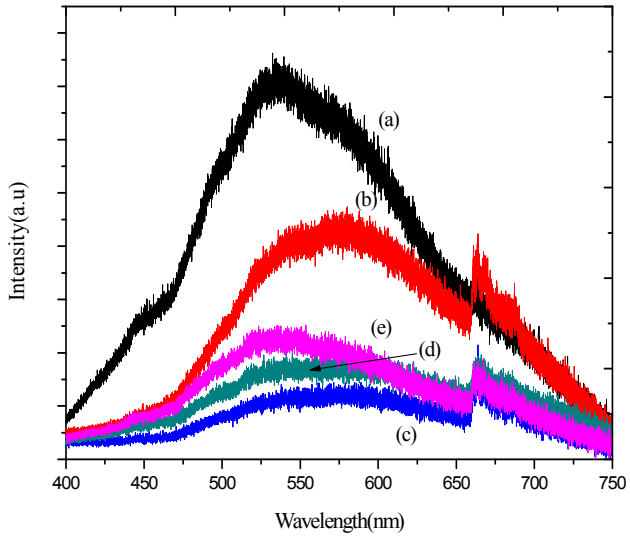

Figure 10. Photoluminescence spectra of $CuTiO_2$NTs (**a**) Cu-00; (**b**) Cu-01; (**c**) Cu-02; (**d**) Cu-03; (**e**) Cu-04.

2.8. Mott-Schottky Analysis

For the purpose of studying the behavior of charge carriers on the Ti substrate interface Mott–Schotkky characterization was performed as shown in Figure 11. The flat band potential was calculated as 0.33 V. A positive slope in the Mott–Schottky revealed that the charge depletion behavior of Ti foil is a n-type photocatalyst material and the higher slope indicates that the substrate surface was covered uniformly. It can be assumed that the charge carriers are predominantly oxygen vacancies. These surface oxygen vacancies can act as catalytic sites for photochemical reactions.

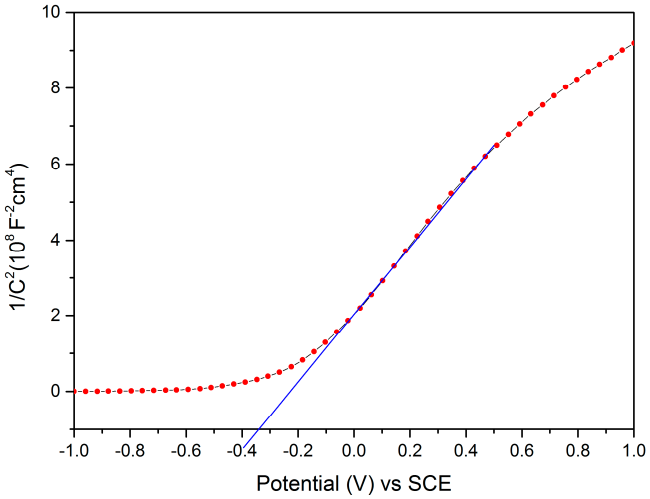

Figure 11. Mott-Schottky analysis of Ti foil at a potential range of −1 to +1 V_{SCE}.

2.9. Simazine Photodegradation Analysis

Using Simazine solution (1 ppm) as the organic pollutant, the photodegradation efficiency of $CuTiO_2$NTs was evaluated. Figure 12 shows the photocatalytic degradation of Simazine solutions over Cu incorporated TiO_2NTs as the photocatalyst, under UV light irradiation. The SMZ solution concentration decreases rapidly with illumination time. The removal efficiency of SMZ incorporated with the optimum Cu loading (0.45 wt %) was 64% in 4 h, while it removed 25% of SMZ for the pure TiO_2NTs sample. The removal efficiency is significantly improved by the addition of Cu element. This confirms the ability of the photocatalyst to degrade persistent organic pollutant. The reasons for this effect can be explained as follows: It was found that the photocatalytic activity of the doped samples is significantly different with pure TiO_2. This significant enhancement can be attributed to the role of Cu in hindering electron-holes recombination taking place thus further improving photocatalytic activity. Furthermore, structural morphologies have significant impact on the photocatalytic activity of $CuTiO_2$NTs. It can be observed that Cu-01 and Cu-03 give a higher efficiency in comparison to Cu-02 due to the reason that the photocatalytic activity is dependent on the structural morphology of the nanotubes with enhanced surface area resulting in an increase of electron transfer ability [41,42]. Cu-01 with the optimum addition amount of Cu is selected to compare the band gap value with a pure-TiO_2 sample labelled Cu-00. In order to study the incorporation effect on optical properties, a comparative UV-Vis diffuse reflectance spectrum of Cu-00 and Cu-01 is shown in Figure 13. Interestingly, the reflectance spectrum shows a slight red shift in optical response as Cu-01 displays greater absorption towards the visible region. This may be a factor that could influence photocatalytic ability [43]. The reflectance was further used to calculate the band gap value of the samples by using a Tauc-Plot. As shown in Figure 14, Cu-01 shows a smaller band gap value, 2.9 eV compared to un-doped TiO_2, 3.1 eV.

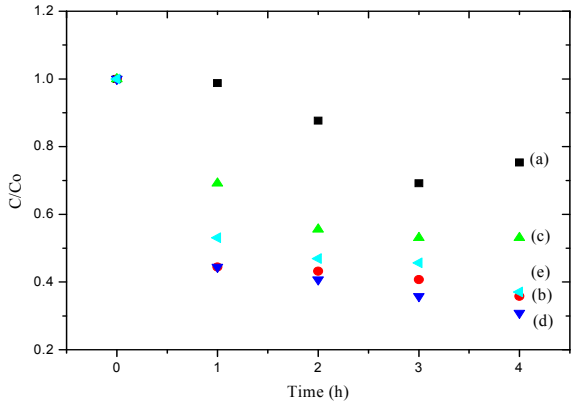

Figure 12. Relationship between C/C_0 and reaction time in hours for Simazine decomposition catalyzed by (**a**) Cu-00; (**b**) Cu-01; (**c**) Cu-02; (**d**) Cu-03; and (**e**) Cu-04 samples under UV irradiation.

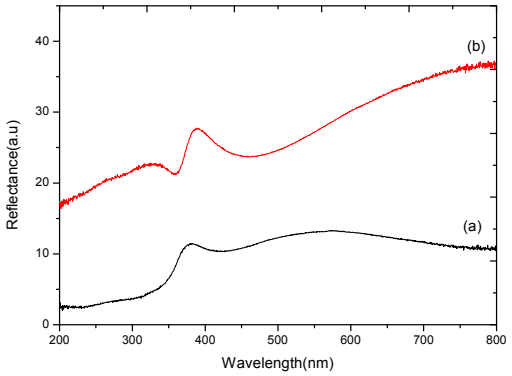

Figure 13. Reflectance vs. wavelength for (**a**) Cu-00 and (**b**) Cu-01.

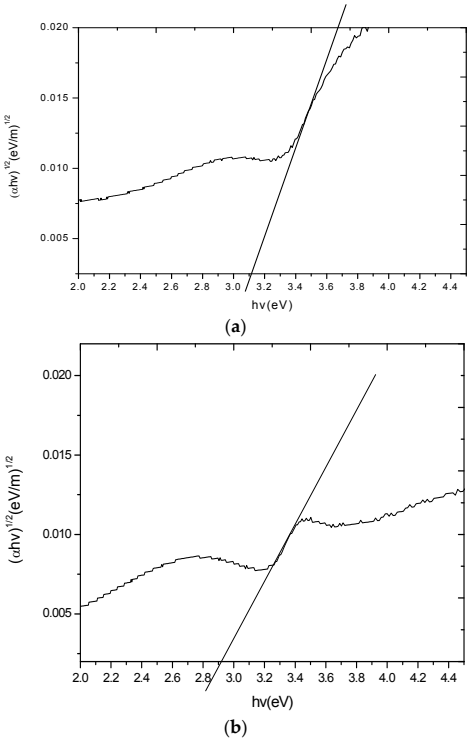

Figure 14. Band gap using Tauc-Plot for sample (**a**) Cu-00 and (**b**) Cu-01.

In addition, the photodegradation efficiency of Cu-02 is significantly weaker than that of any doped samples due to a non-uniform nanotubes morphology resulting in high electron-holes recombination. Table 4 shows the reaction kinetic rate for all samples. It is observed that the sample Cu-03 has the maximum value of percentage of degradation. However, in terms of kinetic rate, the sample Cu-03 shows almost a similar value to the sample Cu-01.

Table 4. Kinetic rate for Simazine decomposition catalyzed by (**a**) Cu-00; (**b**) Cu-01; (**c**) Cu-02; (**d**) Cu-03; and (**e**) Cu-04 samples under UV irradiation.

Sample	Kinetic Rate (h^{-1})
Cu-00	0.0124
Cu-01	0.0135
Cu-02	0.0062
Cu-03	0.0135
Cu-04	0.0106

3. Experimental Techniques

A set of catalysts was prepared via the anodization process as illustrated in Figure 15. Prior to anodization, pure titanium foils (0.127 mm, 99.7% purity (metal basis)) were ultrasonically cleaned in acetone and rinsed with deionized water. TiO_2NTs were fabricated by anodizing Ti sheet as the anode in a two-electrode electrochemical cell with a mixture of Ammonium Fluoride (NH_4F), and EG.

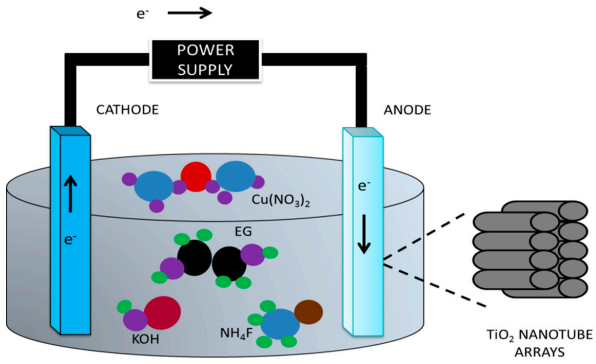

Figure 15. Schematic diagram of experimental setup for catalyst preparation via anodization process, EG = ethylene glycol.

SMZ with molecular weight 206.6 g/mol, and formula $C_7H_{12}ClN_5$, a synthetic compound derived from triazine and used as a herbicide (Figure 16) was supplied by Fluka and used without further treatment. To investigate the effect of Copper loaded TiO_2NTs on SMZ photodegradation ability, Copper(II) nitrate trihydrate [$Cu(NO_3)_2 \cdot 3H_2O$] ranging from 0.45 to 1.80 wt % was added into the mixture of NH_4F, KOH, and EG electrolytes followed by a stirring process. Table 5 shows the details of the parameters.

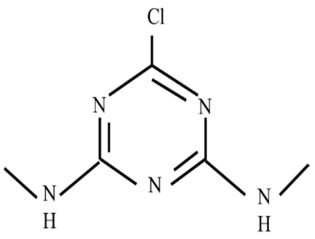

Figure 16. Chemical structure of Simazine.

Table 5. Experimental parameters of the prepared samples.

Label	Fabrication Electrolyte
Cu-00	TiO_2
Cu-01	TiO_2 + Cu (0.45 wt %)
Cu-02	TiO_2 + Cu (0.90 wt %)
Cu-03	TiO_2 + Cu (1.35 wt %)
Cu-04	TiO_2 + Cu (1.80 wt %)

A sample without copper was fabricated in the electrolyte for the control experiment and labelled as Cu-00. Thus the other samples were labelled as Cu-01, Cu-02, Cu-03, Cu-04 for Cu percentage of 0.45%, 0.90%, 1.35%, and 1.80% respectively. The anodization process was performed at 30 V for 30 min for each sample at ambient temperature. After anodization, the Ti sheets were rinsed with deionized water, followed by acetone, dried naturally, and calcinated at 450 °C for 2 h to increase the crystallinity of the TiO_2NTs. The surface morphologies of all samples were examined by Scanning Electron Microscopy (FE-SEM, Quanta 200F, FEI, Germany) and Energy Dispersive X-ray spectroscopy (EDX, Oxford, INCA Software, FEI, Germany) was used for elemental composition characterization. The crystalline characteristics were investigated by X-ray Diffraction (XRD) with Cu Kα radiation. X-ray photoelectron spectroscopy (XPS) measurements were carried out by a scanning X-ray microprobe PHI Quantera II (Ulvac-PHI, INC, Kanagawa, Japan) using a monochromatic Al-K_α (hv = 1486.6 eV) X-ray source that operated at 43.4 W (beam diameter of 300 μm). Wide scan analysis was performed using a pass energy of 280 eV with 1 eV per step for determination of elemental chemical states while narrow scan analysis was performed throughout the binding energy range of interest at a pass energy of 112 eV with 0.1 eV per step. Prior to de-convolution, charge correction was performed at C 1s by setting binding energies of C–C and C–H at 284.8 eV. Raman analysis was performed using In Via Raman Microscope (Renishaw, UK) over the range of 100 cm^{-1} to 700 cm^{-1} at a laser wavelength of 514 nm and 50% of laser power. Samples for Photoluminescence (PL) measurement were irradiated by a monochromatic beam with 325 nm wavelength at room temperature. The PL spectra with an excitation wavelength at 514 nm were recorded in the range of 400 nm to 750 nm. The effect of the TiO_2NTs and the charge transfer behavior was studied by impedance spectroscopy over the TiO_2NT substrates. Electrochemical measurements were done in a three-electrode cell using a platinum wire as counter electrode and a standard Ag/AgCl in 3 M KCl as reference electrode. $[Fe(CN)_6]^{3-/4-}$ solutions were used as electrolyte. Impedance spectra were obtained with an Autolab PGSTAT-302N potentiostat, Metrohm AG, Switzerland) equipped with an impedance analyzer and controlled by a PC. The photoreaction was held under UV-light irradiation with 50 mL of SMZ solution (1 ppm). The source of light was a 95 W UV lamp. The photocatalytic reactor was equipped with 100 mL quartz tubes containing 50 mL of SMZ solutions positioned parallel to the UV source to receive equal light intensity. Cu deposited TiO_2NTs were immersed into SMZ solution in darkness for 30 min, in order for adsorption-desorption to achieve equilibrium. Eventually, the liquid samples were collected every 1 h and analyzed further by UV-Vis analyzer (Varian Cary 50 Series, Agilent Technologies, United States). The band gap energy (Eg) was determined using Tauc/Davis-Mott plot.

4. Conclusions

We demonstrated the degradation of Simazine (SMZ) using Copper (Cu) loaded TiO_2 photocatalyst material in this work. The concentration of Cu plays a significant role in the photocatalytic activity of TiO_2 nanotubes and the optimum concentration for Cu was found as 0.45 wt %. Different crystallinity of TiO_2 nanotubes was also observed with the varying amount of Cu in the catalyst structure. The precise band gap from Mott-Schottky and DR-UV results was derived as 2.9 eV which indicates that the photocatalyst is sufficiently active under near UV-Vis irradiation. Increased kinetic rate of degradation was observed at optimum Cu concentration in TiO_2NTs. These findings show a simple and easy way to degrade SMZ in waste water. Moreover, 1.0

ppm SMZ removal efficiency using 0.45 wt % Cu loaded TiO_2NTs is around 64% in 4 h. This indicates its potential as a fast and reliable photocatalyst in future water treatment applications. Titanium dioxide (TiO_2) owing to its outstanding physical and chemical properties has still the most potential as photocatalyst material in water treatment application.

Acknowledgments: The authors would like to thank the University of Malaya for funding this research work under Fundamental Research Grant Scheme (FRGS: FP008-2015A), Postgraduate Research Fund (PPP: PG034-2013B) and University of Malaya Research Grant (UMRG: RP022-2012A and RP022-2012D).

Author Contributions: Syazwan Hanani Meriam Suhaimy and Chin Wei Lai conceived and designed the experiments; Syazwan Hanani Meriam Suhaimy performed the experiments; Mohd Rafie Johan and Md. Rakibul Hasan analyzed the data; Sharifah Bee Abd Hamid contributed reagents/materials/analysis tools; Syazwan Hanani Meriam Suhaimy wrote the paper.

Conflicts of Interest: The authors declare no conflict of interest.

References

1. Hallberg, G.R. From hoes to herbicides agriculture and groundwater quality. *J. Soil Water Conserv.* **1986**, *41*, 357–364.
2. Rivas, F.; Navarrete, V.; Beltrán, F.J.; García-Araya, J.F. Simazine Fenton's oxidation in a continuous reactor. *Appl. Catal. B Environ.* **2004**, *48*, 249–258. [CrossRef]
3. Sanderson, J.T.; Seinen, W.; Giesy, J.P.; van den Berg, M. 2-Chloro-s-triazine herbicides induce aromatase (CYP19) activity in H295R human adrenocortical carcinoma cells: A novel mechanism for estrogenicity? *Toxicol. Sci.* **2000**, *54*, 121–127. [CrossRef] [PubMed]
4. Chu, W.; Rao, Y.; Hui, W. Removal of simazine in a UV/TiO_2 heterogeneous system. *J. Agric. Food Chem.* **2009**, *57*, 6944–6949. [CrossRef] [PubMed]
5. Evgenidou, E.; Fytianos, K. Photodegradation of triazine herbicides in aqueous solutions and natural waters. *J. Agric. Food Chem.* **2002**, *50*, 6423–6427. [CrossRef] [PubMed]
6. Vanderborght, J.; Tiktak, A.; Boesten, J.J.; Vereecken, H. Effect of pesticide fate parameters and their uncertainty on the selection of 'worst-case'scenarios of pesticide leaching to groundwater. *Pest Manag. Sci.* **2011**, *67*, 294–306. [CrossRef] [PubMed]
7. Sathishkumar, P.; Mangalaraja, R.V.; Mansilla, H.D.; Gracia-Pinilla, M.; Anandan, S. Sonophotocatalytic (42 kHz) degradation of Simazine in the presence of Au–TiO_2 nanocatalysts. *Appl. Catal. B Environ.* **2014**, *160*, 692–700. [CrossRef]
8. Gaya, U.I.; Abdullah, A.H. Heterogeneous photocatalytic degradation of organic contaminants over titanium dioxide: A review of fundamentals, progress and problems. *J. Photochem. Photobiol. C Photochem. Rev.* **2008**, *9*, 1–12. [CrossRef]
9. Zhang, P.; Scrudato, R.J.; Germano, G. Solarcatalytic inactivation of *Escherichia coli* in aqueous solutions using TiO_2 as catalyst. *Chemosphere* **1994**, *28*, 607–611. [CrossRef]
10. Tatsuma, T.; Saitoh, S.; Ohko, Y.; Fujishima, A. TiO_2-WO_3 photoelectrochemical anticorrosion system with an energy storage ability. *Chem. Mater.* **2001**, *13*, 2838–2842. [CrossRef]
11. Yang, T.-Y.; Lin, H.-M.; Wei, B.-Y.; Wu, C.-Y.; Lin, C.-K. UV enhancement of the gas sensing properties of nano-TiO_2. *Rev. Adv. Mater. Sci.* **2003**, *4*, 48–54.
12. Blackwood, D.; Greef, R.; Peter, L. An ellipsometric study of the growth and open-circuit dissolution of the anodic oxide film on titanium. *Electrochim. Acta* **1989**, *34*, 875–880. [CrossRef]
13. López-Muñoz, M.; Aguado, J.; Revilla, A. Photocatalytic removal of s-triazines: Evaluation of operational parameters. *Catal. Today* **2011**, *161*, 153–162. [CrossRef]
14. Wang, M.; Sun, L.; Lin, Z.; Cai, J.; Xie, K.; Lin, C. *p–n* Heterojunction photoelectrodes composed of Cu_2O-loaded TiO_2 nanotube arrays with enhanced photoelectrochemical and photoelectrocatalytic activities. *Energy Environ. Sci.* **2013**, *6*, 1211–1220. [CrossRef]
15. Rao, Y.; Chu, W. Visible Light-Induced Photodegradation of Simazine in Aqueous TiO_2 Suspension. *Ind. Eng. Chem. Res.* **2013**, *52*, 13580–13586. [CrossRef]
16. Mishra, S.; Du, D.; Jeanneau, E.; Dappozze, F.; Guillard, C.; Zhang, J.; Daniele, S. A Facile Molecular Precursor-based Synthesis of Ag_2Se Nanoparticles and Its Composites with TiO_2 for Enhanced Photocatalytic Activity. *Chem. Asian J.* **2016**, *11*, 1658–1663. [CrossRef] [PubMed]

17. Gao, B.; Yap, P.S.; Lim, T.M.; Lim, T.-T. Adsorption-photocatalytic degradation of Acid Red 88 by supported TiO_2: Effect of activated carbon support and aqueous anions. *Chem. Eng. J.* **2011**, *171*, 1098–1107. [CrossRef]
18. Fanun, M. *The Role of Colloidal Systems in Environmental Protection*; Elsevier: Amsterdam, The Netherlands, 2014.
19. Kathalingam, A.; Ambika, N.; Kim, M.; Elanchezhiyan, J.; Chae, Y.; Rhee, J. Chemical bath deposition and characterization of nanocrystalline ZnO thin films. *Mater. Sci. Pol.* **2010**, *28*, 513–522.
20. Krengvirat, W.; Sreekantan, S.; Noor, A.-F.M.; Kawamura, G.; Muto, H.; Matsuda, A. Single-step growth of carbon and potassium-embedded TiO_2 nanotube arrays for efficient photoelectrochemical hydrogen generation. *Electrochim. Acta* **2013**, *89*, 585–593. [CrossRef]
21. Morawski, A.; Grzechulska, J.; Kałucki, K. A new method for preparation of potassium-pillared layered titanate applied in photocatalysis. *J. Phys. Chem. Solids* **1996**, *57*, 1011–1017. [CrossRef]
22. Cai, Q.; Paulose, M.; Varghese, O.K.; Grimes, C.A. The effect of electrolyte composition on the fabrication of self-organized titanium oxide nanotube arrays by anodic oxidation. *J. Mater. Res.* **2005**, *20*, 230–236. [CrossRef]
23. Raymundo-Pinero, E.; Azais, P.; Cacciaguerra, T.; Cazorla-Amorós, D.; Linares-Solano, A.; Béguin, F. KOH and NaOH activation mechanisms of multiwalled carbon nanotubes with different structural organisation. *Carbon* **2005**, *43*, 786–795. [CrossRef]
24. Heldebrant, D.J.; Jessop, P.G. Liquid poly(ethylene glycol) and supercritical carbon dioxide: A benign biphasic solvent system for use and recycling of homogeneous catalysts. *J. Am. Chem. Soc.* **2003**, *125*, 5600–5601. [CrossRef] [PubMed]
25. Luo, C.; Zhang, Y.; Zeng, X.; Zeng, Y.; Wang, Y. The role of poly(ethylene glycol) in the formation of silver nanoparticles. *J. Colloid Interface Sci.* **2005**, *288*, 444–448. [CrossRef] [PubMed]
26. Ghicov, A.; Schmuki, P. Self-ordering electrochemistry: A review on growth and functionality of TiO_2 nanotubes and other self-aligned MO*x* structures. *Chem. Commun.* **2009**, 2791–2808. [CrossRef] [PubMed]
27. Chaudhary, V.; Srivastava, A.K.; Kumar, J. On the Sol-gel Synthesis and Characterization of titanium oxide nanoparticles. In Proceedings of the MRS Spring Meeting and Exhibit, San Francisco, CA, USA, 25–29 April 2011; Cambridge Univsity Press: Cambridge, UK, 2011.
28. Zhang, J.; Li, M.; Feng, Z.; Chen, J.; Li, C. UV Raman spectroscopic study on TiO_2. I. Phase transformation at the surface and in the bulk. *J. Phys. Chem. B* **2006**, *110*, 927–935. [CrossRef] [PubMed]
29. Di Valentin, C.; Pacchioni, G.; Selloni, A.; Livraghi, S.; Giamello, E. Characterization of paramagnetic species in N-doped TiO_2 powders by EPR spectroscopy and DFT calculations. *J. Phys. Chem. B* **2005**, *109*, 11414–11419. [CrossRef] [PubMed]
30. Sarra-Bournet, C.; Haberl, B.; Charles, C.; Boswell, R. Characterization of nanocrystalline nitrogen-containing titanium oxide obtained by N_2/O_2/Ar low-field helicon plasma sputtering. *J. Phys. D Appl. Phys.* **2011**, *44*, 455202. [CrossRef]
31. Chen, X.; Liu, L.; Peter, Y.Y.; Mao, S.S. Increasing solar absorption for photocatalysis with black hydrogenated titanium dioxide nanocrystals. *Science* **2011**, *331*, 746–750. [CrossRef] [PubMed]
32. Lazarus, M.; Sham, T. X-ray photoelectron spectroscopy (XPS) studies of hydrogen reduced rutile (TiO_2-*x*) surfaces. *Chem. Phys. Lett.* **1982**, *92*, 670–674. [CrossRef]
33. Biesinger, M.C.; Lau, L.W.; Gerson, A.R.; Smart, R.S.C. Resolving surface chemical states in XPS analysis of first row transition metals, oxides and hydroxides: Sc, Ti, V, Cu and Zn. *Appl. Surf. Sci.* **2010**, *257*, 887–898. [CrossRef]
34. Ding, J.; Yuan, Y.; Xu, J.; Deng, J.; Guo, J. TiO_2 nanopowder Co-doped with iodine and Boron to enhance visible-light photocatalytic activity. *J. Biomed. Nanotechnol.* **2009**, *5*, 521–527. [CrossRef] [PubMed]
35. Kandjani, A.E.; Sabri, Y.M.; Periasamy, S.R.; Zohora, N.; Amin, M.H.; Nafady, A.; Bhargava, S.K. Controlling core/shell formation of nanocubic p-Cu_2O/n-ZnO toward enhanced photocatalytic performance. *Langmuir* **2015**, *31*, 10922–10930. [CrossRef] [PubMed]
36. Pauly, N.; Tougaard, S.; Yubero, F. Determination of the Cu 2p primary excitation spectra for Cu, Cu_2O and CuO. *Surf. Sci.* **2014**, *620*, 17–22. [CrossRef]
37. Li, G.; Dimitrijevic, N.M.; Chen, L.; Rajh, T.; Gray, K.A. Role of surface/interfacial Cu^{2+} sites in the photocatalytic activity of coupled CuO^{-} TiO_2 nanocomposites. *J. Phys. Chem. C* **2008**, *112*, 19040–19044. [CrossRef]

38. Zhang, W.; Zou, L.; Lewis, R.; Dionysio, D. A Review of Visible-Light Sensitive TiO_2 Synthesis via Sol-Gel *N*-Doping for the Degradation of Dissolved Organic Compounds in Wastewater Treatment. *J. Mater. Sci. Chem. Eng.* **2014**, *2*, 28.
39. Kumar, M.K.; Bhavani, K.; Srinivas, B.; Kumar, S.N.; Sudhakar, M.; Naresh, G.; Venugopal, A. Nano structured bismuth and nitrogen co-doped TiO_2 as an efficient light harvesting photocatalyst under natural sunlight for the production of H_2 by H_2O splitting. *Appl. Catal. A Gen.* **2016**, *515*, 91–100. [CrossRef]
40. Memesa, M.; Lenz, S.; Emmerling, S.G.; Nett, S.; Perlich, J.; Müller-Buschbaum, P.; Gutmann, J.S. Morphology and photoluminescence study of titania nanoparticles. *Colloid Polym. Sci.* **2011**, *289*, 943–953. [CrossRef] [PubMed]
41. Hafez, H.; Lan, Z.; Li, Q.; Wu, J. High efficiency dye-sensitized solar cell based on novel TiO_2 nanorod/nanoparticle bilayer electrode. *Nanotechnol. Sci. Appl.* **2010**, *3*, 45–51. [CrossRef] [PubMed]
42. Pavasupree, S.; Ngamsinlapasathian, S.; Nakajima, M.; Suzuki, Y.; Yoshikawa, S. Synthesis, characterization, photocatalytic activity and dye-sensitized solar cell performance of nanorods/nanoparticles TiO_2 with mesoporous structure. *J. Photochem. Photobiol. A Chem.* **2006**, *184*, 163–169. [CrossRef]
43. Park, H.; Park, Y.; Kim, W.; Choi, W. Surface modification of TiO_2 photocatalyst for environmental applications. *J. Photochem. Photobiol. C Photochem. Rev.* **2013**, *15*, 1–20. [CrossRef]